Journal of Biological Regulators and Homeostatic Agents 2026, 40(3), 122.
https://doi.org/10.65746/jbrha122

Article

Lung cancer severity detection with pulmonary pathology using optimized deep learning framework

Albert Punitha Jilt[1,*], Govindasamy Kavitha[2]

[1] Department of Computer Science and Engineering, St. Anne's College of Engineering and Technology, Anguchettyplayam, Panruti 607106, Tamilnadu, India
[2] Department of Computer Science and Engineering, Muthayammal Engineering College (Autonomous), Rasipuram, Namakkal 637408, Tamilnadu, India
*** Corresponding author:** Albert Punitha Jilt, srjiltsat@stannescet.ac.in

CITATION

Punitha Jilt A, Kavitha G. Lung cancer severity detection with pulmonary pathology using optimized deep learning framework. Journal of Biological Regulators and Homeostatic Agents. 2026; 40(3): 122.
https://doi.org/10.65746/jbrha122

ARTICLE INFO

Received: 7 May 2026
Revised: 29 May 2026
Accepted: 3 June 2026
Available online: 9 June 2026

Abstract: Lung cancer leads to mortality worldwide, and hence, accurate cancer grading is essential for prognosis and treatment planning. Existing tumor grading approaches are time-consuming and prone to inter-observer inconsistency. Also, existing Deep Learning (DL) approaches focus on binary classification and fail to identify the fine-grained tumor aggressiveness, which is crucial for accurate prognosis and treatment planning. This study develops a hybrid attention-based DL grading framework for accurate detection and grading of lung cancer into adenocarcinoma, squamous cell carcinoma, and normal tissues, which differentiates into grade 1, grade 2, and grade 3 tumor grades. The proposed methodology utilizes a Macenko color normalization method to preprocess the high-resolution histopathological images. The proposed work introduces a hybrid attention-based DL framework, ResCBAM-ViTFSG, that integrates ResNet18 with Convolutional Block Attention Module (CBAM) for extracting local spatial features and Vision Transformer with Feature Selection Gate (FSG) for extracting global features. To improve robustness, introduced a novel Uncertainty-Aware Reweighting Adam (UAR-Adam) optimizer that dynamically adjusts learning rates. The proposed work achieved fine-grained grading of lung cancer through per-class grading analysis, effective feature extraction counts, and optimizer benchmarking, achieving an accuracy of 98.34 %, precision of 98.50 %, recall of 98.18 %, F1-score of 98.34 %, and an inference time of 7.8 ms. These results outperform baseline models in lung cancer grading, suitable for deployment in pulmonary pathology clinical diagnostic systems.

Keywords: deep learning; histopathological images; lung cancer grading; pulmonary pathology; uncertainty-aware reweighted Adam.

1. Introduction

Lung cancer is the leading cause of malignant tumors worldwide, with a high morbidity and mortality rate [1]. The 2023 statistics estimated 238,340 lung cancer cases in the United States, presenting a serious public health issue [2]. Lung cancer is separated into two types based on pathological characteristics: Small Cell Lung Carcinoma (SCLC), which represents microscopic glandular-related tissue cytology, and Non-Small Cell Lung Carcinoma (NSCLC), which denotes the observable traits of squamous differentiation, which includes 80–85% of lung cancer cases. The NSCLC types are lung adenocarcinoma (ADC) and lung squamous cell carcinoma (LUSC) [3,4]. Early detection of pulmonary pathology is vital for refining the survival rate of patients with lung cancer [5]. Histopathological images are the most significant method for diagnosing lung cancer subtypes, providing information on the structure

of tissues and cells, and enabling pathologists to identify and classify tumors [6,7]. Recently, tumor grading has played an important part in the diagnosis of lung cancer in pathology. Tumor grading is an important component in the pathologic diagnosis of lung cancer, which assesses the tumor aggressiveness, treatment decision, and prognosis [8]. The grading of ADC and LUSC follows the grading criteria by the International Association for the Study of Lung Cancer (IASLC) that suggests a three-tier grading system: low grade, intermediate grade, and high grade. According to the IASLC grading criteria, Grade 1 tumors are considered low-grade and are characterized by a lepidic growth pattern and which has no high-grade features. Grade 2 tumors are classified as intermediate-grade and commonly exhibit papillary or acinar growth patterns with less than 20 % high-grade components, indicating moderate tumor aggressiveness [9,10]. Grade 3 tumors are categorized as high-grade they contain more than 20 % high-grade features such as solid or micropapillary patterns, which are strongly associated with rapid tumor progression, poor prognosis, and increased metastatic potential [11,12]. This grading system helps pathologists assess tumor severity and supports more accurate clinical decision-making and treatment planning.

Recent advancements in pulmonary pathology leverage Deep Learning (DL) approaches for cancer cell detection. Tan et al. [13] evaluated the IASLC grading system for predicting the Recurrence Specific Survival (RSS) and Lung Cancer Specific Survival (LCSS) for stage 1 patients with ADC. The approach splits the grade 2 tumors and accurately stratifies tumors by prognosis. Niedermaier et al. [14] proposed a study to evaluate the low-grade patterns in patients with intermediate-grade and high-grade ADC at the pathological stage. These results, the low grade showed no prognostic significance in intermediate and high-grade non-mucinous ADC. Elazab et al. [15] presented a system for accurately grading tumors by analyzing histopathological images. The model utilized YOLO for object detection and ResNet for feature extraction to support pathologists in reducing variability in manual grading. Li et al. [16] developed a model for lung cancer subtype classification through advanced DL Models to analyze complex histopathological features. The model utilized the Support Vector Machines (SVMs) to classify the lung cancer types from the extracted features. However, the model only included the initial stage of lung cancer histopathological images. Sethy et al. [17] proposed a hybrid model for the lung cancer classification through histopathological images. The framework combined AlexNet, Wavelet, and SVMs to classify the lung cancer into three categories such as benign, ADC, and LUSC. Sumon et al. [18] proposed a hybrid model using DenseNet-121 for feature extraction and combined several Machine Learning (ML) classifiers. The model provided a solution to assist pathologists in early lung cancer diagnosis.

The primary issues with these works are that the current tumor grading methods are based on the manual histopathological evaluation of tumor patterns, and also that most available pathology approaches consider only binary classifications and fail to capture the finer differentiation grades that are clinically essential for risk stratification. Additionally, traditional lung cancer approaches struggle to extract local cellular features and global tissue in high-resolution histopathological images. To overcome these issues, we introduce a DL-based grading framework to classify ADC and LUSC into clinically relevant grades: grade 1, grade 2, and grade 3, based on their

aggressiveness from histopathological images, and this is intended to enhance the reproducibility, efficacy, and prognostic accuracy of lung cancer grading. The major contributions of the proposed work are outlined below:

- The study develops a hybrid attention-based DL framework for the accurate detection and grading of lung cancer into ADC, LUSC, and normal tissue to support early diagnosis and treatment planning in pulmonary pathology.
- We have developed a ResCBAM-ViTFSG model that integrates ResNet18 with the Convolutional Block Attention Module (CBAM) to enhance local features in histopathological images. We also improvised the vision transformer (ViT) by adding the Feature Selection Gate (FSG) attention layer to capture global features and long-range dependencies.
- We have developed an Uncertainty-Aware Reweighted Adam (UAR-Adam) optimizer to adjust the learning rate based on staining variability, ambiguous tissue regions, and inter-observer disagreement uncertainties to ensure the generalization of the model.

The remaining portion of this paper is structured as follows. Section II defined the methodology of the proposed framework. Section III delivers the experimental results, and Section IV includes the conclusion of the work.

2. Materials and methods

The proposed hybrid attention-based DL framework for lung cancer grading is illustrated in **Figure 1**. We initially preprocessed the raw lung cancer high-resolution histopathological images through resizing. Macenko color normalization method is used to enhance image quality, and then we used data augmentation to increase the diversity of the dataset. The dual-branch ResCBAM-ViTFSG model integrates enhanced ResNet18 with the CBAM model to extract the global features, and ViT with FSG to extract the global features. Then, both features are fused and fed into the Monte Carlo Dropout with the developed UAR-Adam optimizer to reweight the learning rate based on uncertainty captured by dropout to ensure reliable predictions. Finally, the images are fed into the classification head of the ResNet18, which contains a SoftMax layer and a Fully Connected (FC) layer to grade the lung cancer into tumor grades based on their aggressiveness.

2.1. Dataset description of LungHist700 dataset

The LungHist700 dataset [19] includes the high-resolution lung histopathological images of 691 collected from 45 patients. The dataset contains adenocarcinoma, squamous cell carcinoma, and normal tissues that are split into three different levels based on aggressiveness. The dataset is split into 70 % for model training, 20 % for validation, and 10 % for testing. **Figure 2** shows the sample images. In **Table 1**, based on the guidelines of IASLC, lung cancer is graded into three different levels based on the tumor aggressiveness. Grade 1 means a lepidic pattern that has no high-grade features. Grade 2 shows papillary patterns that have less than twenty percentage high-grade features, and Grade 3 includes more than 20 % high-grade features.

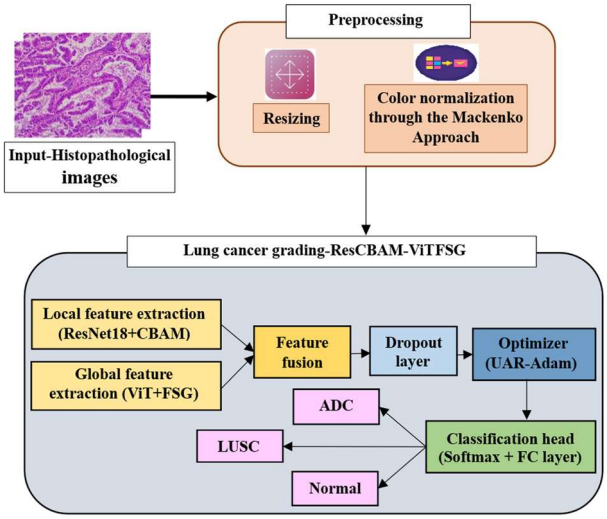

Figure 1. Schematic diagram of the proposed hybrid attention-based deep learning framework for lung cancer grading.

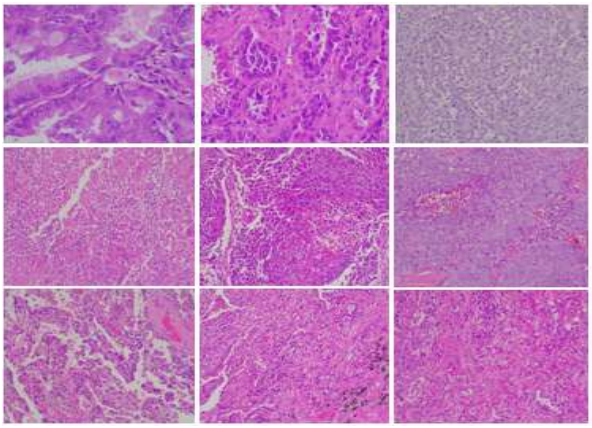

Figure 2. Sample images from the LungHist700 dataset. The first row indicates the ADC with different tumor differentiation, and the second row represents the LUSC with different tumor differentiation. The last row indicates the normal lung tissue images.

Table 1. Categorization of malignant tumors based on their aggressiveness.

Description	Total samples	Training samples (70 %)	Validation samples (20 %)	Testing samples (10 %)
ADC grade 1	103	72	21	10
ADC grade 2	90	63	18	9
ADC grade 3	87	61	17	9
LUSC grade 1	50	35	10	5
LUSC grade 2	30	21	6	3
LUSC grade 3	48	34	9	5
Normal	151	106	30	15
Total	691	484	111	56

2.2. Histopathological image preprocessing

The LungHist700 histopathological images undergo a preprocessing phase, including resizing and color normalization to normalize the input data. Resizing is used to adjust images in a constant dimension for effective model training. The input images are resized into a 224 × 224-dimension pixels, aligning with the proposed model's requirements. Then, the image is applied to the color normalization to improve the image features. For color normalization, the Macenko method [20] is utilized to convert the color space of the image to a new color space, which splits the stain from the non-stain information. This normalization process effectively reduces inter-slide staining variability caused by differences in tissue preparation, staining protocols, and scanning conditions across histopathological slides. Macenko normalization standardizes the chromatic profiles of the images, ensuring consistent colour distributions and improving the robustness of feature extraction during model training. Then, data augmentation is performed to enhance the diversity of the dataset by flipping and rotating the histopathological images. The preprocessed histopathological image is shown in **Table 2**.

Table 2. Preprocessed images of adenocarcinoma, normal, and squamous cell carcinoma lung tissues.

	ADC	**Normal**	**LUSC**
Input image	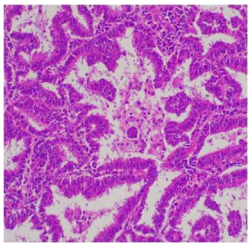	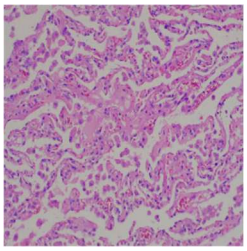	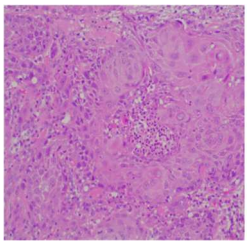
Preprocessed image	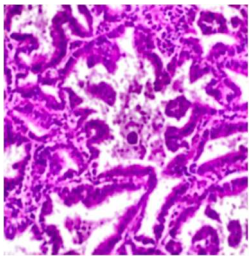	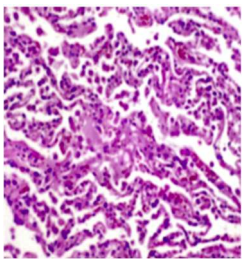	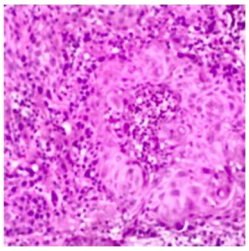

2.3. Lung cancer grading through ResCBAM-ViTFSG

We introduce a dual-branch hybrid DL framework, ResCBAM-ViTFSG for lung cancer grading that combines ResNet-18 with CBAM and an enhanced ViT block with the FSG to effectively grade lung cancer using histopathological images. The backbone ResNet18 layer with CBAM extracts local features, and the ViT block with an FSG layer extracts global features, fuses them onto the Monte Carlo Dropout layer to capture predictive uncertainty. The developed UAR-Adam optimizer reweights the learning rate based on uncertainty. Finally, the classification head, which includes a softmax and FC layers, grades the lung cancer. **Figure 3** shows the architecture diagram of the ResCBAM-ViTFSG grading framework. The architecture of ResNet-18, features a sequence of convolutional blocks that use average pooling for input processing and output generation. This network comprises eight residual building

blocks and 17 convolutional layers, a 3 × 3 max pooling layer, and a FC layer.

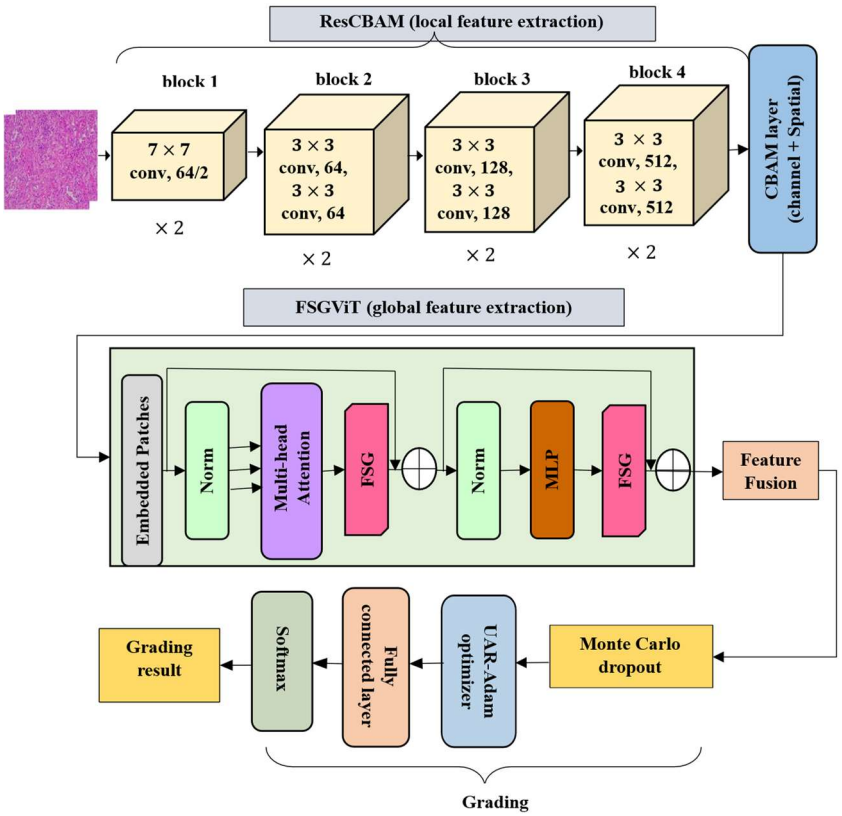

Figure 3. Architecture diagram of the dual-branch ResCBAM-ViTFSG framework.

ResNet18 model incorporates a ReLU activation function and Batch Normalization (BN) following all convolution layers. The two primary attention modules in CBAM are the channel attention module and the spatial attention module. The channel attention captures the weights across various channels to enhance their correlations, and the spatial attention focuses on learning weights among different locations to improve spatial relationships. The integrated ResNet18 with CBAM architecture extracts local features from lung histopathological images. Each ResNet18 residual block includes two convolutional layers. We embed CBAM within each ResNet residual block of the neural network structure. This enriches intermediate feature maps, converting them into vital information that represents the input. The ResNet18-CBAM branch extracts local spatial feature representations in multidimensional tensor form. To enable feature fusion, the extracted spatial feature maps are flattened and refined into a compact one-dimensional feature vector representation. Simultaneously, the ViT-FSG branch generates a global contextual feature embedding that captures long-range dependencies and semantic tissue information. Before concatenation, both feature representations are dimensionally aligned through feature refinement and transformation operations to ensure compatibility along the feature axis. The aligned local and global feature vectors are then concatenated to form the final fused feature representation used for lung cancer grading. The feature fusion process can be represented as expressed in Equation (1).

$$F_{\text{fusion}} = \text{Concat}(F_{\text{ResCBAM}}, F_{\text{ViT-FSG}}) \quad (1)$$

Where, F_{ResCBAM} represents the refined local morphological features extracted from the ResNet18-CBAM branch and $F_{\text{ViT-FSG}}$ denotes the global contextual feature embedding generated by the ViT-FSG branch. This fusion strategy enables effective integration of local tissue characteristics and global contextual dependencies for robust histopathological grading performance. After feature extraction, both local and global features are concatenated subsequently and passed to the UAR-Adam optimizer before SoftMax to estimate prediction uncertainty. After feature fusion, we employed the Monte Carlo Dropout (MCD) layer to reduce model complexity and avoid overfitting. It also supports more reliable and transparent decision-making in lung cancer grading.

2.4. Enhanced UAR-Adam optimizer

In lung cancer grading, the training samples often vary in confidence because low-contrast or noisy images may lead to inefficient grading. The proposed enhanced Adam optimizer, Uncertainty-Aware Reweighted Adam (UAR-Adam), improves the baseline Adam by ensuring more stable training and improved generalization, thereby preventing aggressive updates on uncertain samples. The Adam optimizer is defined using Equation (2).

$$A_{\mathfrak{t}} = Z_{\mathfrak{t}-1} - \mu \frac{\widehat{\mathfrak{m}_{\mathfrak{t}}}}{\sqrt{\widehat{\mathbb{v}}_{\mathfrak{t}} + \epsilon}} \tag{2}$$

Where $\mathbb{W}_{\mathfrak{t}}$ is updated at each step based on previous values, learning rate μ, and gradient estimates $\mathfrak{m}_{\mathfrak{t}}$ and $\mathbb{v}_{\mathfrak{t}}$. We introduced the uncertainty-scaled learning rate used to adjust the learning based on the predicted uncertainty. It's defined using Equation (3):

$$\mu_{\mathfrak{i}} = \mu_0 \cdot (1 - \sigma_{\mathfrak{i}}) \tag{3}$$

Where $\sigma_{\mathfrak{i}}$ is the uncertainty estimate for the sample $\mathfrak{i}$, calculated using MCD. To estimate predictive uncertainty, MCD is employed during inference by maintaining active dropout layers and performing multiple stochastic forward passes for the same histopathological image. The predicted probability distributions obtained from these stochastic passes are utilized to compute the predictive mean and variance. The uncertainty σ_i is estimated as the variance of the predicted class probabilities across the Monte Carlo samples, as denoted in Equation (4).

$$\sigma_{\mathfrak{i}} = \text{Var}(p_i^{(1)}, p_i^{(2)}, \dots, p_i^{(N)}) \tag{4}$$

Where, $p_i^{(k)}$ denotes the predicted probability obtained from the k^{th} stochastic forward pass and N represents the total number of Monte Carlo samples used during inference. Now, we replaced the baseline Adam optimizer's learning rate with the developed uncertainty-scaled learning rate. As we have named, UAR-Adam optimizer, replaces the baseline optimizer's usage with a dynamic pre-sample learning rate scaled by uncertainty. The UAR-Adam optimizer is given in Equation (5):

$$A_{\mathfrak{t}} = Z_{\mathfrak{t}-1} - \mu_{\mathfrak{i}} \frac{\widehat{\mathfrak{m}_{\mathfrak{t}}}}{\sqrt{\widehat{\mathbb{v}}_{\mathfrak{t}} + \epsilon}} \tag{5}$$

Where $\mu_{\mathfrak{i}}$ represents the uncertainty-scaled learning rate. This enhancement makes

training of lung cancer grading more efficient, scaling down the learning rate for high-uncertainty samples and making the optimizer aware of model confidence. Finally, the images are fed into the classification head, which contains a softmax layer and an FC layer to grade the cancer using the lung histopathological images.

3. Results and discussion

3.1. Implementation environment and hyperparameter selection

The proposed framework performed using a workstation equipped with an NVIDIA Quadro M200 GPU with 16 GB RAM, and an Intel Core i7 processor. The proposed ResCBAM-ViTFSG framework was implemented using the python 3.10 version. During both training and inference, a batch size of 32 was used.

For the implementation process, image size of 224 × 224 is used and the data augmentation process flipped with 0.5 value and rotated with ±30 ° to improve the diversity of the dataset. A batch size of 32 entries at an initial learning rate of 0.001. **Table 3** illustrates the hyperparameters of the proposed hybrid attention-based DL framework, including learning rate, epoch, optimizer, and attention details.

The hyperparameters in **Table 3** represent the proposed model's performance and generalizability while minimizing overfitting. The selected hyperparameters improved training convergence, regularization to reduce overfitting, and enhanced model generalization capacity.

Table 3. Hyperparameter selection of the proposed model.

Component	Hyperparameters	Value
ResNet-18 backbone	Pretrained	True
	Output shape	(B, 2048, 7, 7)
Attention modules	Channel attention reduction	16
	Spatial attention kernel size	7
ViT backbone	Pretrained	True
	Head	Identity
	Output shape	(B, 768)
Feature fusion	Concatenated feature dim	2048 × 7× 7 + 768 = 10640
	FC1 in features	10,640
	FC1 out features	512
	Activation function	ReLU
	Dropout rate	0.3
	FC2 out features	3
	final activation	SoftMax

Table 3. (*Continued*).

Component	Hyperparameters	Value
Training	Epochs	30
	Learning rate	1e-4
	Optimizer	UAR-Adam
	Scheduler	Cosine annealing
	Loss function	Cross entropy

3.2. Performance analysis of the proposed hybrid DL-based grading framework

Table 4 illustrates the performance of the lung cancer grading using the metrics accuracy, precision, recall, and F1-score. The proposed model performed well in both the tumor and normal cases with a high accuracy. This highlights the proposed hybrid DL-based framework's effectiveness in tumor grading.

Table 4. Performance evaluation of the proposed model based on the tumor aggressiveness.

Class	Grading	Accuracy (%)	Precision (%)	Recall (%)	F1-score (%)
Adenocarcinoma	Grade 1	98.60	98.75	98.50	98.63
	Grade 2	98.10	98.60	98.00	98.30
	Grade 3	97.85	98.25	98.10	98.18
Normal	Normal	99.20	99.00	98.90	98.95
Squamous cell carcinoma	Grade 1	97.90	98.10	97.50	97.80
	Grade 2	98.30	98.35	98.20	98.28
	Grade 3	98.45	98.50	98.10	98.30
Average		98.34	98.50	98.18	98.34

3.3. Layer-wise results of the proposed dual-branch ResCBAM with ViT-FSG model

This section presents the layer-wise experimental outcomes of the proposed ResCBAM with the ViT-FSG model. This result explains how the model grades lung cancer using the histopathological lung images. This illustrates the experimental portions, including ResNet-18 (stem Layer), ResNet-18 (Tail Layer), CBAM, and ViT-FSG. The obtained outcomes are represented in **Figure 4**.

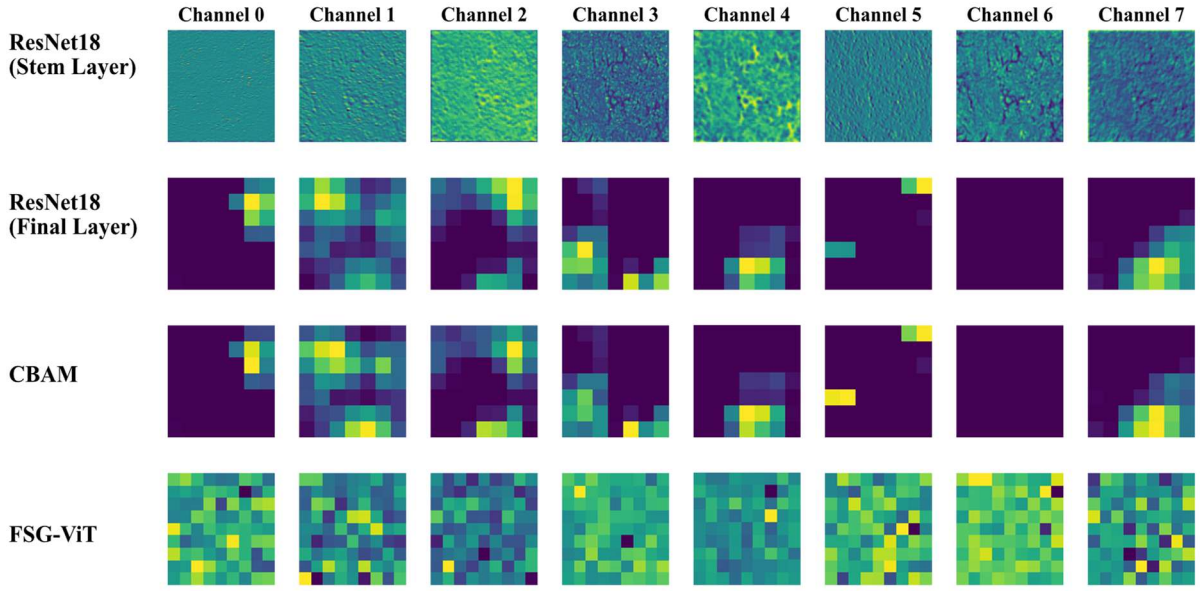

Figure 4. Layer-wise results of the proposed ResCBAM-ViTFSG model for lung cancer grading. Row1: Local morphological feature extraction obtained from the ResNet18 stem layers. Row 2: Deeper local discriminative feature representations extracted from the ResNet18 tail layers. Row 3: Feature maps generated through the CBAM module. Row 4: Global contextual feature representations extracted using the ViTFSG branch.

3.4. Extracted feature counts from the LungHist700 dataset

Table 5 presents the per-class extracted feature counts obtained from the LungHist700 dataset using the proposed hybrid attention-based DL framework. Each image in the dataset generates local features through the ResNet18 + CBAM branch and extracts global features through the ViT + FSG branch. After fusion, this results in combined fused features as represented in the table. Across all seven grades, the average extracted features are listed in the table below. The feature extraction process is uniformly distributed across classes, ensuring that no category is underrepresented during model training. By combining local cellular-level details and global context such as tissue-level structures, the fused representation achieves a balanced and discriminative feature set. This uniformity enhances the generalization capability of the model, reducing class imbalance bias and strengthening its ability to accurately grade tumors across all differentiation levels.

Table 5. Features extracted from each class of the dataset.

Lung cancer grade	No. of images	ResNet18 + CBAM (Local features Avg norm)	ViT + FSG (global features Avg norm)	Fused features (Avg norm)
ADC-grade 1	103	145.28	84.13	169.48
ADC-grade 2	90	129.58	84.14	157.17
ADC-grade 3	87	88.11	84.14	123.71
Normal	151	122.94	84.13	149.78
LUSC-grade 1	99	161.79	84.16	184.27
LUSC-grade 2	66	97.90	84.14	130.27
LUSC-grade 3	95	118.89	84.15	147.15
Total	691	125.37	84.14	153.11

3.5. Analysis of the proposed enhanced optimizer UAR-Adam

Figure 5 shows the calibration curve which assesses how well a model forecast probabilities align with real results, which is particularly crucial in clinical diagnosis. In this study, we used Monte Carlo Dropout for uncertainty estimation and the UAR-Adam optimizer for uncertainty-aware training. This results in well-calibrated probability scores, where the predicted confidence levels more accurately reflect true classification likelihoods. shows the calibration curve for the proposed model. This reflects improved model calibration facilitated by UAR-Adam, which enhances the trustworthiness and clinical applicability of the model's predictions. We experimented with the proposed UAR-Adam optimizer with different Standard optimizers like Adamax, RMS Prop, SGD, and Nadam to evaluate the impact on accuracy. The proposed UAR-Adam incorporates uncertainty estimation in weight updates.

This analysis shows that the proposed UAR-Adam outperforms other optimizers, indicating that uncertainty awareness leads to a more stable optimization path, benefiting our lung cancer grading task. The proposed UAR-Adam optimizer with diverse epochs and learning rates confirm the proposed model's performance, as shown in **Table 6**. This shows how the proposed UAR-Adam optimizer improves the model's performance.

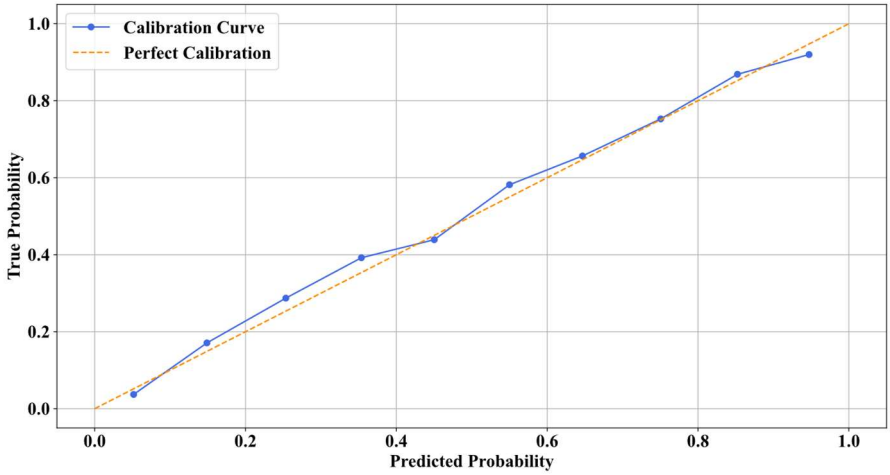

Figure 5. Proposed UAR-Adam optimizer's calibration curve.

Table 6. Evaluation performance of the proposed hybrid attention-based DL model with different optimizers based on varied epochs and learning rate values.

Optimizer	Epochs	Learning rate	Accuracy (%)	Precision (%)	Recall (%)	F1-score (%)
Adamax	10	0.001	95.40	94.30	93.70	94.00
	20	0.001	95.90	94.80	94.10	94.50
	30	0.001	96.20	95.10	94.50	94.80
RMS Prop	10	0.0005	95.80	94.90	94.20	94.60
	20	0.0005	96.20	95.20	94.50	94.80
	30	0.0005	96.50	95.45	94.70	95.07
SGD	10	0.0006	94.10	93.10	92.30	92.60
	20	0.0006	94.70	93.50	92.80	93.10
	30	0.0006	95.10	94.00	93.20	93.60

Table 6. (*Continued*).

Optimizer	Epochs	Learning rate	Accuracy (%)	Precision (%)	Recall (%)	F1-score (%)
Nadam	10	0.0005	96.30	95.50	95.10	95.20
	20	0.0005	96.70	95.80	95.40	95.60
	30	0.0005	97.00	96.10	95.80	95.95
Proposed (UAR-Adam)	10	0.0001	98.01	98.10	97.95	98.20
	20	0.0001	98.08	98.20	98.05	98.05
	30	0.0001	98.34	98.50	98.18	99.34

3.6 Generalization performance of the proposed model with the LC25,000 dataset

Table 7 presents the performance of the proposed model across the LC25,000 dataset [21]. The dataset includes 25,000 histopathological images with five classes. This analyzes the proposed model's performance on another histopathological lung cancer image dataset. It represents our proposed model is generalized better across another dataset. The validation of our model through the external dataset emphasizes its clinical pathologists' decision-making.

Table 7. Generalization performance of the proposed model.

Dataset split	Class	Accuracy (%)	Precision (%)	Recall (%)	F1-score (%)
Train and Validation	Lung adenocarcinoma	98.85	98.70	98.60	98.65
	Lung normal	98.82	98.60	98.50	98.55
	Lung squamous cell carcinoma	98.88	98.75	98.70	98.72
	Average	98.85	98.68	98.60	98.64
Testing	Lung adenocarcinoma	98.65	98.40	98.20	98.30
	Lung normal	98.58	98.30	98.10	98.20
	Lung squamous cell carcinoma	98.70	98.50	98.40	98.45
	Average	98.64	98.40	98.23	98.32

3.7. Ablation study

This section analyzes the improved performance of each module of our proposed hybrid attention-based DL framework and the optimizer performance for lung cancer grading. The baseline ResNet18 model attained a lower grading performance than the proposed hybrid model. The proposed ResCBAM-ViTFSG attained a superior performance with an accuracy of 98.34 %, precision of 98.50 %, recall of 98.18 %, and a F1-score of 98.34 %. This highlights the importance of the proposed hybrid attention-based DL model in lung cancer grading, as represented in **Table 8**.

Table 8. Ablation study analysis.

Model	Accuracy (%)	Precision (%)	Recall (%)	F1-score (%)
ResNet18	95.60	94.50	94.10	94.30
ResNet18 + CBAM	96.80	95.70	95.30	95.50
ResNet18 + ViT	97.10	96.00	95.60	95.80
ResNet18 + FSG	96.90	95.90	95.40	95.60

Table 8. (*Continued*).

Model	Accuracy (%)	Precision (%)	Recall (%)	F1-score (%)
ResNet18 + CBAM + ViT	98.20	97.10	96.80	96.95
ResNet18 + CBAM + FSG	98.50	97.30	97.00	97.15
Without UAR - Adam optimizer	96.20	95.80	95.12	96.43
Proposed (ResCBAM-ViTFSG)	98.34	98.50	98.18	98.34

3.8. Comparison of proposed model with baseline approaches

Table 9 represents a detailed comparison between the proposed hybrid attention-based DL framework and different baseline models for the grading of pulmonary pathology. The proposed hybrid attention-based DL model performs better than all the baseline models, achieving the highest accuracy of 98.34 %, precision of 98.50 %, recall of 98.55 %, specificity of 99.45 %, and F1-score of 98.34 %. Remarkably, baseline models ResNet34, Xception, and InceptionV3 exhibited better performance; they struggle to achieve a balance between specificity.

ResNet50 achieved a high specificity showing a tendency to grade pulmonary pathology. Additionally, the lightweight baseline models swin transformer, ViT, and VGG19 performed poorly compared to our proposed model. The parameter count analysis demonstrates that the proposed ResCBAM - ViTFSG framework contains a moderately higher number of trainable parameters due to the integration of attention mechanisms and transformer-based global feature extraction, it achieves significantly superior grading performance while maintaining a clinically feasible inference time of 7.8 ms. This indicates an effective balance between computational complexity and diagnostic accuracy compared with existing CNN-based architectures. The superior performance of the proposed hybrid attention-based DL framework proves its architectural improvements and supports its suitability for deployment in pulmonary pathology clinical diagnostic systems.

Table 9. Comparison of the proposed model with different baseline models

Model	Params (M)	Accuracy (%)	Precision (%)	Recall (%)	Specificity (%)	F1-Score (%)	Inference Time (ms)
ResNet34	21.80	95.84	95.91	95.72	95.79	95.81	12.84
Xception	22.91	96.27	96.34	96.18	96.21	96.26	14.21
InceptionV3	23.85	95.73	95.81	95.62	95.69	95.71	13.76
ResNet50	25.56	96.58	96.64	96.51	96.47	96.57	15.34
Swin transformer	28.30	96.42	96.56	96.35	96.38	96.41	16.82
ViT	86.00	97.11	97.18	97.03	97.08	97.10	24.53
VGG19	143.67	94.89	95.01	94.72	94.81	94.86	31.68
Proposed (ResCBAM with ViT-FSG)	12.48	98.34	98.50	98.18	98.45	98.34	7.8

4. Conclusion

This study successfully developed a hybrid attention-based DL framework for lung cancer tumor grading. The proposed ResCBAM-ViTFSG framework

demonstrates strong potential as an intelligent decision-support system for pulmonary pathology by enabling reliable and fine-grained lung cancer grading from histopathological images. The ResCBAM-ViTFSG framework integrated ResNet18 with the CBAM for enhanced extraction of local spatial features, allowing the model to capture fine cellular-level details critical for differentiating tumor grades. The proposed system to effectively capture clinically relevant tumour characteristics highlights its potential for supporting early diagnosis, improving grading consistency, and facilitating personalized treatment planning in pulmonary oncology. The proposed framework resulted in a balanced and discriminative feature representation that enhanced robustness across adenocarcinoma, squamous cell carcinoma, and normal tissue, while capturing clinically relevant grading levels (grades 1, 2, and 3). This ensures the proposed hybrid attention-based DL framework is a robust, interpretable, and computationally effective solution for fine-grained lung cancer grading, paving the way for deployment in pulmonary pathology diagnostic systems.

Despite the promising grading performance achieved by the proposed ResCBAM - ViTFSG framework, this study has some limitations. First, the LungHist700 dataset contains only 691 histopathological images collected from a limited number of patients, which may restrict the overall diversity of tissue morphology patterns available during training. The dataset does not include multi-centre histopathological slides with diverse staining protocols and scanner variations. Additionally, rare lung cancer subtypes and uncommon pathological patterns are underrepresented in the dataset, limiting the model's ability to generalize across all pulmonary pathology cases. Future work will focus on conducting prospective multi-centre validation studies using histopathological datasets collected from diverse clinical institutions to further evaluate the robustness and generalizability of the proposed framework. Furthermore, future extensions of this work will investigate the integration of histopathological image features with patient clinical metadata, including demographic information, genomic biomarkers, and treatment history, to enable more comprehensive prognostic stratification and personalized treatment decision-making in pulmonary oncology.

Author contributions: Conceptualization, APJ and GK; methodology, APJ; software, APJ; validation, APJ, GK; formal analysis, APJ; investigation, APJ; resources, GK; data curation, GK; writing original draft preparation, GK; writing review and editing, APJ; visualization, GK; supervision, GK; project administration, APJ; funding acquisition, GK. All authors have read and agreed to the published version of the manuscript.

Funding: None.

Ethical approval: Not applicable.

Informed consent statement: Not applicable.

Conflict of interest: The authors declare no conflict of interest.

References

1. Wankhade S, Vigneshwari S. A novel hybrid deep learning method for early detection of lung cancer using neural networks. Healthcare Analytics. 2023; 3(1): 100195. doi: 10.1016/j.health.2023.100195

2. Noaman NF, Kanber BM, Al Smadi A, et al. Advancing oncology diagnostics: AI-enabled early detection of lung cancer through hybrid histological image analysis. IEEE Access. 2024; 12(3): 64396–64415. doi: 10.1109/ACCESS.2024.3397040
3. Li M, Ma X, Chen C, et al. Research on the auxiliary classification and diagnosis of lung cancer subtypes based on histopathological images. IEEE Access. 2021; 9(2): 53687–53707. doi: 10.1109/ACCESS.2021.3071057
4. Wang L. Deep learning techniques to diagnose lung cancer. Cancers. 2022; 14(22): 5569. doi: 10.3390/cancers14225569
5. Mridha MF, Prodeep AR, Hoque AM, et al. A comprehensive survey on the progress, process, and challenges of lung cancer detection and classification. Journal of Healthcare Engineering. 2022; 2022(1): 5905230. doi: 10.1155/2022/5905230
6. Rajasekar V, Vaishnnave MP, Premkumar S, et al. Lung cancer disease prediction with CT scan and histopathological images feature analysis using deep learning techniques. Results in Engineering. 2023; 18(5): 101111. doi: 10.1016/j.rineng.2023.101111
7. Zhang Y, Yang Z, Chen R, et al. Histopathology images-based deep learning prediction of prognosis and therapeutic response in small cell lung cancer. NPJ Digital Medicine. 2024; 7(1): 15. doi: 10.1038/s41746-024-01003-0
8. Diosdado J, Gilabert P, Seguí S, Borrego H. LungHist700: A dataset of histological images for deep learning in pulmonary pathology. Scientific Data. 2024; 11(1): 1088. doi: 10.1038/s41597-024-03944-3
9. Rokutan-Kurata M, Yoshizawa A, Ueno K, et al. Validation study of the International Association for the Study of Lung Cancer histologic grading system of invasive lung adenocarcinoma. Journal of Thoracic Oncology. 2021; 16(10): 1753–1758. doi: 10.1016/j.jtho.2021.04.008
10. Han YB, Kim H, Mino-Kenudson M, et al. Tumor spread through air spaces (STAS): Prognostic significance of grading in non-small cell lung cancer. Modern Pathology. 2021; 34(3): 549–561. doi: 10.1038/s41379-020-00709-2
11. Fujikawa R, Muraoka Y, Kashima J, et al. Clinicopathologic and genotypic features of lung adenocarcinoma characterized by the international association for the study of lung cancer grading system. Journal of Thoracic Oncology. 2022; 17(5): 700–707. doi: 10.1016/j.jtho.2022.02.005
12. Moreira AL, Ocampo PS, Xia Y, et al. A grading system for invasive pulmonary adenocarcinoma: A proposal from the International Association for the Study of Lung Cancer Pathology Committee. Journal of Thoracic Oncology. 2020; 15(10): 1599–1610. doi: 10.1016/j.jtho.2020.06.001
13. Tan KS, Reiner A, Emoto K, et al. Novel insights into the international association for the study of lung cancer grading system for lung adenocarcinoma. Modern Pathology. 2024; 37(7): 100520. doi: 10.1016/j.modpat.2024.100520
14. Niedermaier B, Rolf E, Allgäuer M, et al. Prognostic impact of lepidic growth in intermediate and high-grade lung adenocarcinoma. Lung Cancer. 2025; 206(5): 108674. doi: 10.1016/j.lungcan.2025.108674
15. Elazab N, Gab-Allah WA, Elmogy M. A multi-class brain tumor grading system based on histopathological images using a hybrid YOLO and RESNET networks. Scientific Reports. 2024; 14(1): 4584. doi: 10.1038/s41598-024-54864-6
16. Li M, Ma X, Chen C, et al. Research on the auxiliary classification and diagnosis of lung cancer subtypes based on histopathological images. IEEE Access. 2021; 9(1): 53687–53707. doi: 10.1109/ACCESS.2021.3071057
17. Sethy PK, Geetha Devi A, Padhan B, et al. Lung cancer histopathological image classification using wavelets and AlexNet. Journal of X-Ray Science and Technology. 2023; 31(1): 211–221. doi: 10.3233/xst-221301
18. Sumon RI, Mazumdar MAI, Uddin SMI, et al. Exploring deep learning and machine learning techniques for histopathological image classification in lung cancer diagnosis. 2024 International Conference on Electrical, Computer and Energy Technologies ICECET. IEEE; 2024. pp. 1–6. doi: 10.1109/ICECET61485.2024.10698211
19. LungHist700 dataset. Available online: https://www.kaggle.com/datasets/abdullahhasansajjad/lunghist700 (accessed on 5 February 2026).
20. Rehman ZU, Wan Ahmad WSHM, Ahmad Fauz, et al. Comprehensive analysis of color normalization methods for HER2-SISH histopathology images. Journal of Engineering Science and Technology. 2024; 19(2): 146–159.
21. LC25,000 dataset. Available online: https: // www.kaggle.com/datasets/javaidahmadwani/lc25,000 (accessed on 5 February 2026).